Geophysical Journal International

Geophys. J. Int. (2015) **201,** 823–837
GJI Geodynamics and tectonics

doi: 10.1093/gji/ggv053

The seismogenic structure of the 2013–2014 Matese seismic sequence, Southern Italy: implication for the geometry of the Apennines active extensional belt

L. Ferranti,[1] G. Milano,[2] P. Burrato,[3] M. Palano[4] and F. Cannavò[4]

[1] *Dipartimento di Scienze della Terra, delle Risorse e dell'Ambiente, Università Federico II, Largo S. Marcellino* 10, *I*-80138 *Napoli, Italy.*
E-mail: lferrant@unina.it
[2] *Istituto Nazionale di Geofisica e Vulcanologia, Osservatorio Vesuviano, Via Diocleziano* 328, *I*-80124 *Napoli, Italy*
[3] *Istituto Nazionale di Geofisica e Vulcanologia, Via di Vigna Murata,* 605, *I*-00143 *Roma, Italy*
[4] *Istituto Nazionale di Geofisica e Vulcanologia, Osservatorio Etneo, Piazza Roma* 2, *I*-95123 *Catania, Italy*

Accepted 2015 February 2. Received 2015 February 1; in original form 2014 November 14

SUMMARY

Seismological, geological and geodetic data have been integrated to characterize the seismogenic structure of the late 2013-early 2014 moderate energy (maximum local magnitude $M_{Lmax} = 4.9$) seismic sequence that struck the interior of the Matese Massif, part of the Southern Apennines active extensional belt. The sequence, heralded by a $M_L = 2.7$ foreshock, was characterized by two main shocks with $M_L = 4.9$ and $M_L = 4.2$, respectively, which occurred at a depth of ∼17–18 km. The sequence was confined in the 10–20 km depth range, significantly deeper than the 1997–1998 sequence which occurred few km away on the northeastern side of the massif above ∼15 km depth. The depth distribution of the 2013–14 sequence is almost continuous, albeit a deeper (16–19 km) and a shallower (11–15 km) group of events can be distinguished, the former including the main shocks and the foreshock. The epicentral distribution formed a ∼10 km long NNW–SSE trending alignment, which almost parallels the surface trace of late Pliocene–Quaternary southwest-dipping normal faults with a poor evidence of current geological and geodetic deformation. We built an upper crustal model profile for the eastern Matese massif through integration of geological data, oil exploration well logs and seismic tomographic images. Projection of hypocentres on the profile suggests that the seismogenic volume falls mostly within the crystalline crust and subordinately within the Mesozoic sedimentary cover of Apulia, the underthrust foreland of the Southern Apennines fold and thrust belt. Geological data and the regional macroseismic field of the sequence suggest that the southwest-dipping nodal plane of the main shocks represents the rupture surface that we refer to here as the Matese fault. The major lithological discontinuity between crystalline and sedimentary rocks of Apulia likely confined upward the rupture extent of the Matese fault. Repeated coseismic failure represented by the deeper group of events in the sequence, activated in a passive fashion the overlying ∼11–15 km deep section of the upper crustal normal faults. We consider the southwest-dipping Matese fault representative of a poorly known type of seismogenic structures in the Southern Apennines, where extensional seismogenesis and geodetic strain accumulation occur more frequently on NE-dipping, shallower-rooted faults. This is the case of the Boiano Basin fault located on the northern side of the massif, to which the 1997–1998 sequence is related. The close proximity of the two types of seismogenic faults at the Matese Massif is related to the complex crustal architecture generated by the Pliocene–early Pleistocene contractional and transpressional tectonics.

Key words: Seismicity and tectonics; Continental tectonics: extensional; Crustal structure.

1 INTRODUCTION

The axial belt of the Southern Apennines is characterized by active extension, which is accommodated by a swarm of normal faults located in the high part of the mountain chain. These faults are responsible for large ($M \sim 7$) historical (Fig. 1) and instrumental earthquakes. Valuable parametric information and inference on the geometry of the seismogenic faults were provided by the moment magnitude $M_w = 6.9$, 1980 earthquake, which was caused by slip on the ∼60° northeast-dipping Irpinia fault (Fig. 1;

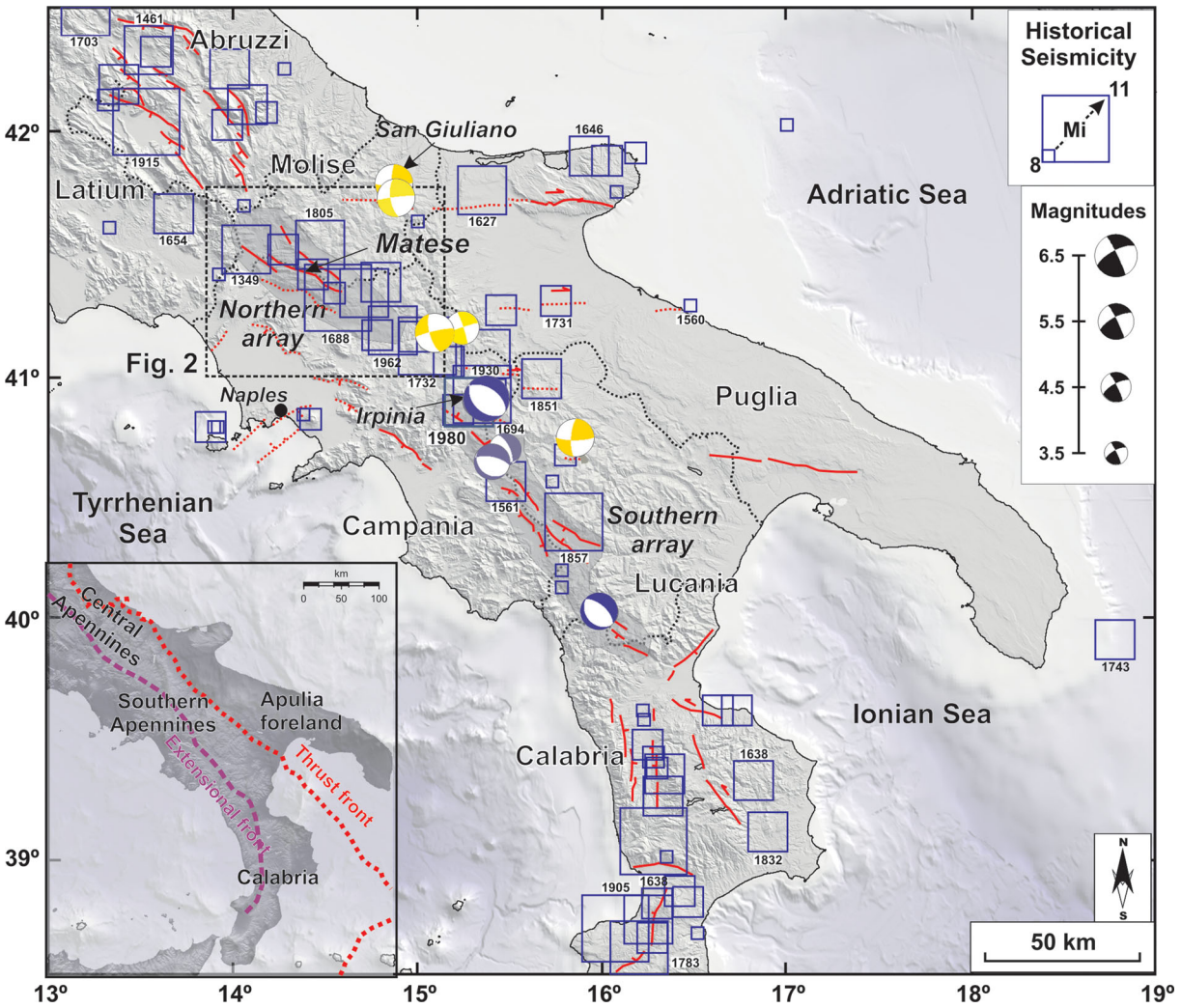

Figure 1. Regional seismotectonic map of southern Italy. Blue squares are historical earthquakes from CPTI11 Catalogue (Rovida *et al.* 2011); Mi, Macroseismic intensity. Active faults are shown with red lines, dotted when inferred. Focal mechanisms of significant recent seismic events are also reported (redrawn from Ferranti *et al.* 2014, with references). Inset shows the generalized position of the extensional and thrust fronts in the Apennines.

Westaway & Jackson 1987; Pantosti & Valensise 1990). Other northeast-dipping faults are part of the active extensional array and are in many cases associated to individual historical earthquakes (DISS Working Group 2010). These faults are thought to extend down to ∼15 km of depth, which is commonly the maximum nucleation depth of moderate and large events of the last ∼35 yr.

SW-dipping faults are also included in the belt and some of them have accommodated a large geological extension, with formation of intermountain and coastal basins (Fig. 1). However, the seismogenic potential for the southwest-dipping faults is still poorly established because, although possibly associated to some destructive historical earthquakes that occurred west of the Apennines crest, large events have not occurred on these faults in the instrumental era.

During late 2013-early 2014 a moderate energy seismic sequence (M_L < 5.0), which lasted nearly a month, struck the internal part of the Matese Massif, the major mountain range of the Campania-Molise segment of the Apennines (Fig. 1). No evidence of active faulting has been recorded so far in the interior of the massif, but the epicentral area of the sequence is aligned amidst the macroseismic epicentral sectors of the destructive M_w = 6.6, 1349 (9 September) and M_w = 7.0, 1688 events (Fig. 2).

In this contribution, we propose a characterization of the seismogenic structure responsible for the seismic sequence by using an integrated seismological, geological and geodetic investigation. Because this study documents that the Matese sequence has nucleated at a depth greater than the one typical of the instrumental seismicity in the Apennines, it underscores that a different, and so far poorly understood type of seismogenic structures may exist west of the well-known extensional belt straddling the mountain crest.

At a more local scale, the 2013–2014 sequence highlights the location of an unknown seismogenic source nested between faults responsible of destructive historical events. Thus, efforts in constraining the geometry and crustal properties of the causative fault for the sequence may offer a critical contribution to seismic hazard evaluation of the region.

2 SEISMOTECTONIC SETTING

2.1 Crustal architecture and active deformation

Quaternary extension has affected the western part of the Southern Apennines and has been accommodated by NW–SE striking normal faults which crosscut the pre-existing thrust structures (Hyppolite

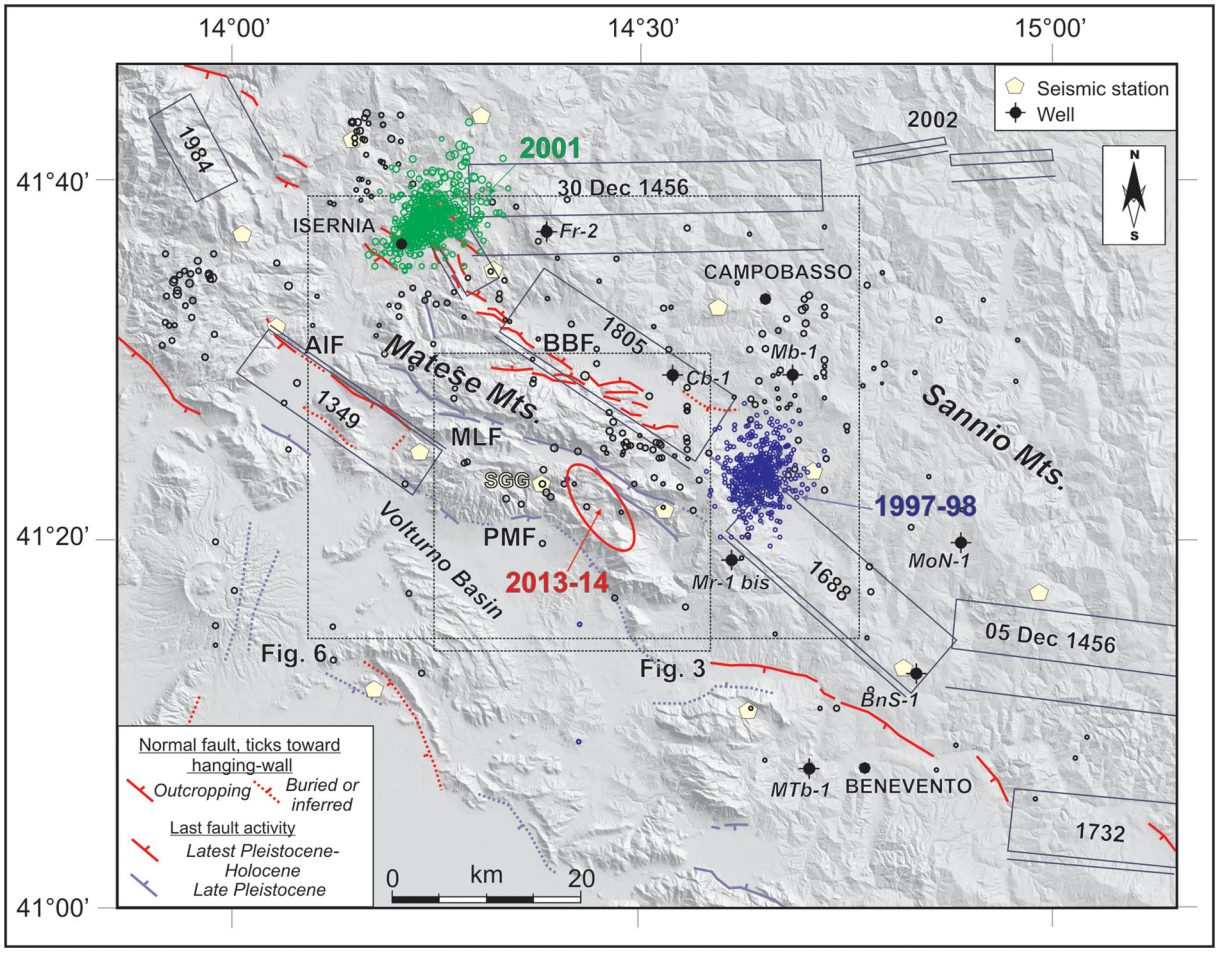

Figure 2. Active faults, seismogenic sources and instrumental seismicity since 1996 in the Sannio-Matese area. Black circles for sparsely seismic events, green and blue for the 1997–1998 and 2001 seismic sequences (Milano *et al.* 2008; Fracassi & Milano 2014). The epicentral distribution of the 2013–14 seismic sequence is indicated by a solid red ellipse. Individual seismogenic sources considered responsible for historical (years inside the source) earthquakes are shown with rectangles (DISS Working Group 2010). Fault (Ferranti *et al.* 2014): AIF, Acquae Iuliae fault; BBF, Boiano Basin fault; MLF, Matese Lake fault; PMF Piedimonte Matese Fault. Wells used in this study: Mb-1, Mirabello 1; FR-2, Frosolone 2; Cb-1, Campobasso 1; Mr-1bis, Morcone 1 bis; MoN-1, Molinara Nord 1; BnS-1, Benevento Sud 1; MTb-1, Monte Taburno 1.

et al. 1994; Ferranti & Oldow 2005). Extension has been related to a combination of backarc rifting in the Tyrrhenian Sea basin west of the Apennines (Fig. 1; Patacca *et al.* 1990), and to excess potential energy resulting from uplift driven by crustal or subcrustal processes (Doglioni *et al.* 1996; Ferranti *et al.* 2014).

Today, extensional active faults and seismicity are concentrated within a ∼40-km-wide belt which runs along the mountain ridge (Fig. 1). Within this belt, upper crustal earthquakes exhibit focal mechanisms with ∼NE–SW trending tensile axis, roughly orthogonal to the chain (Pondrelli *et al.* 2011). Seismological observations are generally consistent with borehole breakouts (Montone *et al.* 2012), fault-slip data from Quaternary rocks (Hyppolite *et al.* 1994; Maschio *et al.* 2005; Papanikolaou & Roberts 2007) and geodetic velocities (Palano *et al.* 2011; D'Agostino 2014; Ferranti *et al.* 2014).

Within the northern part of the Southern Apennines, the strongest historical seismicity is concentrated around the Matese Massif (Figs 1 and 2). The mountain range forms a rectangular block which stretches 30 km ∼NW–SE and 10 km ∼NE–SW, and is floored by Mesozoic–Cenozoic carbonate platform and minor siliciclastic rocks (D'Argenio *et al.* 1973). Regional geological analysis (Patacca & Scandone 2007), along with published seismic sections interpretation and exploration well logs in the area surrounding the massif (Mostardini & Merlini 1986; Casero *et al.* 1988; Calabrò *et al.* 2003; Di Bucci *et al.* 2005a) indicate that the Matese carbonate platform rocks are thrust above coeval basin carbonate and terrigenous rocks of the Molisan (or Sannio-Molisan) thrust assemblage, extensively exposed to the east. The Molisan basin rocks in turn rest structurally above Mesozoic–Cenozoic carbonate platform rocks which are the westward continuation of the Apulia platform exposed further to the east in the foreland of the Apennines (inset in Fig. 1). The buried platform rocks are themselves affected by minor shortening, possibly involving their crystalline basement (Calabrò *et al.* 2003; Di Bucci *et al.* 2005a).

The present structure of the Matese Massif is the result of Quaternary motion on NW–SE striking extensional faults superposed onto earlier thrust and transpressional deformation (Ferranti 1997; Calabrò *et al.* 2003). Locally, the normal faults were reactivated in oblique motion with ∼NW–SE trending tensile axis (Ferranti 1997).

Faults with evidence of recent and possibly active motion are mapped along the flanks of the massif. A NE-dipping normal fault system (Boiano Basin fault, BBF, Fig. 2) forms the northeastern border of Matese (Di Bucci *et al.* 2005b). The fault has middle Pleistocene–Holocene activity (Galli & Galadini 2003), and is

considered responsible for the $M_w = 6.6$, 1805 earthquake (Fig. 2; DISS Working Group 2010).

On the west side of the massif, the southwest-dipping Acquae Iuliae fault (Fig. 2) is viewed as the source of large historical and prehistorical earthquakes, including the 9 September $M_w \sim 6.6$, 1349 event (Galli & Naso 2009). East of Matese, a $M_w \sim 7.0$ earthquake occurred in 1688 (Fig. 2), however its seismogenic structure has not been unquestionably identified (see discussion in Di Bucci *et al.* 2005a).

The southwestern boundary of the massif is represented by a southwest-dipping normal fault (Piedimonte Matese fault; hereinafter PMF), which uplifts the range relative to the Volturno Basin (Fig. 2). Throw of up to ∼1–2 km on this fault is suggested by a deep gravimetric anomaly centred upon the basin (Calabrò *et al.* 2003).

The internal part of the massif is dissected by the southwest-dipping Matese Lake fault (MLF), which borders the northern side of a linear, >30-km-long asymmetric basin (Fig. 2). The fault is suspected to have slipped during the Holocene (Bousquet *et al.* 1993; Galadini *et al.* 2000), but a clear geomorphic evidence of this activity is lacking.

2.2 Instrumental seismicity

Although struck by destructive historical events (Fig. 2) with Macroseismic Intensity Mi > X, the region centred around the Matese Massif is characterized also by small instrumental seismic activity. Milano *et al.* (2008) and Fracassi & Milano (2014) showed that seismicity occurred in the region during 1997–2011 is constituted by independent events, generally with $M < 3.0$, typically 2.5, and hypocentres within the upper 15 km of the crust. These events prevalently align NW–SE along the axis of the chain, and are consistent with the regional NE-SW trending extension as documented by their focal mechanisms.

Low magnitude seismic sequences and swarms are superimposed to this background seismicity. Pertinent examples are the 1997–1998 ($M < 4.2$) and 2001 ($M < 3.6$) sequences (Fig. 2; see Milano *et al.* 2002, 2005 for details on these sequences) and the low-magnitude swarms ($M < 3.2$), lasting few days and consisting of some tens of events, occurred in 1999, 2000, 2005 and 2010.

In contrast to the background seismicity, the 1997–1998 and 2001 seismic sequences cluster at the eastsoutheast and westnorthwest lateral tips, respectively, of the 1805 seismogenic source on the northern side of the massif (Fig. 2). The sequences align along NNE–SSW to NE–SW trends and, as shown by computed focal mechanisms and stress analysis, are related to a local NW–SE extensional stress.

With respect to the restricted area in which the Matese Massif is located, with the exclusion of the 1997–1998 and 2001 seismic sequences, only few isolated events with $M < 3.0$ and hypocentres in the first 20 km of the crust, occurred without a preferred alignment in the time period 2006–2011 (see fig. 4 in Milano *et al.* 2008). In particular, seismicity is almost absent in the limited area where the 2013–2014 sequence occurred.

3 DATA AND METHODS

3.1 Seismic data and location of the events

The sequence started on 2013 December 29 (17:08 UTC) with a $M_L = 4.9$ shock and was characterized by an intense seismic activity till the first week of January, 2014. The main shock was immediately preceded by an event with $M_L = 2.7$ (17:03 UTC). A second shock ($M_L = 4.2$) occurred on 2014 January 20 (7:12 UTC), and, in turn, was followed by low-magnitude seismic activity till January 23. Seismicity totally ceased afterwards. Details on the temporal evolution of the sequence can be found in De Gori *et al.* (2014).

The largest MCS intensities (VI–VII) were located towards the Volturno basin, which flanks the massif to the SW (Fig. 3; Convertito *et al.* 2014). The main shocks were felt in a vast area prevalently to the south of the Matese Massif. In particular, they were felt in Naples and on the conterminous Tyrrhenian sea margin ∼80 km away from the epicentral area.

For this study, we used seismic data recorded by the Italian Telemetered Seismic Network (ITSN) operated by Istituto Nazionale di Geofisica e Vulcanologia (INGV) and consisting of more than 300 stations. The present-day ITSN configuration ensures a fairly good azimuthal coverage of the Italian territory and allows locating also low-magnitude events ($M_L \leq 2$). We also used data from the OV-INGV seismic network (including station SGG which is located only 5 km away from the epicentral area (Fig. 2), and data from two seismic stations belonging to the INGV Mobile Network installed in the epicentral area in the hours following the main shock (De Gori *et al.* 2014).

Following the approach used in previous seismotectonic studies in the area (e.g. Milano *et al.* 2008) we performed a number of trials designed to estimate the reliability of earthquake location taking into consideration the number and quality of *P* and *S* pickings, the azimuthal coverage of the seismic stations around the seismogenic volume and the velocity model adopted. All seismic stations in the area of the sequence are three-component and the nearest permanent one is SGG (Fig. 2). We then focused on the quality of *P* and *S* pickings and on the velocity model. First, we collected digital waveforms of the recorded data related to the 2013–2014 seismic sequence and performed a repicking of the events, focusing our attention on *S*-phase for the reliability of the focal depth. Successively, for location purposes we selected events recorded by a minimum of five stations and with at least five *P*- and four *S*-phase readings.

To estimate the dependence of earthquake location from the velocity model, we performed several location trials on events with variable number of recordings, both few and many. Seismic events have been located by means of the standard HYPO71 algorithm (Lee & Lahr 1975) utilizing the few available velocity models for the area (Chiarabba & Amato 1996; Chiarabba & Frepoli 1997; Iannaccone *et al.* 1998; Milano *et al.* 1999), with a trial focal depth of 10 km. By utilizing only data of seismic stations within a radius of ∼50 km, the trials performed showed no significant differences among the earthquake locations parameter. On the contrary, by incorporating also data of seismic stations >50 km from the epicentral area, the velocity model of Milano *et al.* (1999) shows the highest stability of earthquake locations parameters because it minimizes both the residuals and the relative errors, particularly for the depth of the events. Therefore the Milano *et al.* (1999) velocity model, which was used for localizing the 1997–1998 sequence events (Milano *et al.* 2002), has been adopted for this study (Table 1), The V_P/V_S ratio was obtained by trial-and-error procedure resulting in a value of 1.78. Maximum error location on horizontal position and depth is 2.0 km; maximum rms value is 0.45 s.

Further trials have been performed by using the HYPOELLIPSE location code (Lahr 1999). In particular, we performed some tests utilizing differentiated velocity model. We obtained, however, a general worsening of the locations parameter because detailed crustal

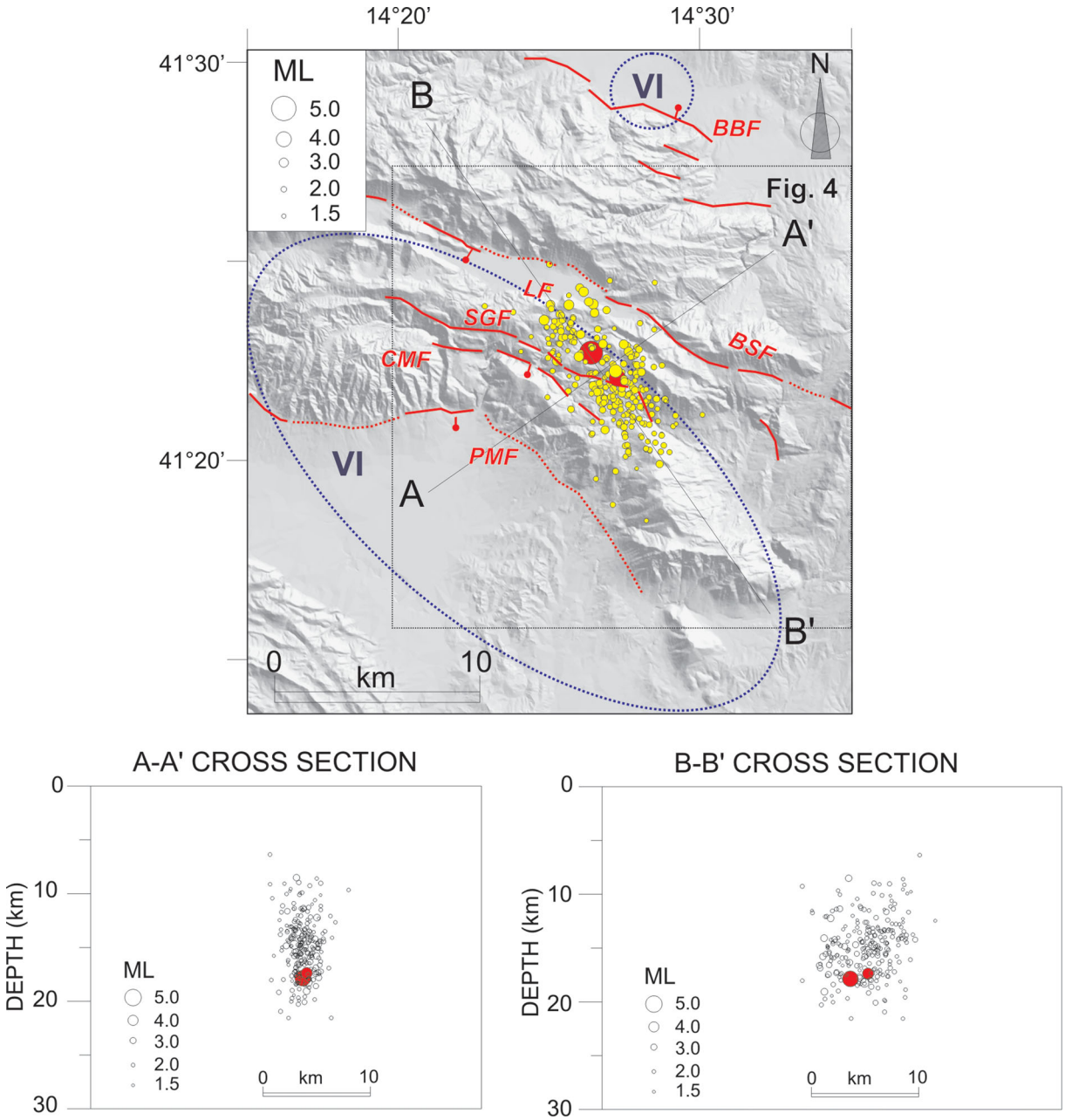

Figure 3. Epicentral (top) and hypocentral (bottom) distribution of earthquakes occurred during the 2013–2014 seismic sequence. The dotted blue ellipse includes the areas with MCS intensities VI–VII (from Convertito *et al.* 2014). Red circles indicate the location of the main shocks ($M_L = 4.9$, 2013 December 29; and $M_L = 4.2$, 2014 January 20). Fault: BBF, Boiano Basin fault; MLF; BSF, Bocca della Selva fault; CMF, Castello Matese fault; LF, Lake fault; PMF Piedimonte Matese fault; SGF, San Gregorio fault.

Table 1. Velocity model adopted in this study (Milano *et al.* 1999).

V_P	Depth
4.5	0.0
5.5	2.0
5.8	10.0
6.7	23.0
8.2	35.0
8.3	50.0

velocity information at a regional scale for the area surrounding Matese is not available.

The comparison between location parameters obtained with HYPO71 and HYPOELLIPSE, utilizing the velocity model of Milano *et al.* (1999), shows consistent results, confirming the quality and stability of the locations. Only for about 15 events (about 7 per cent of the data set) we obtained a general improvement of the locations parameter by using the HYPOELLIPSE code whereas only a small improvement is obtained for the remaining events. Therefore, the final earthquake locations have been performed using the HYPOELLIPSE code. About 95 per cent of the earthquakes are of quality A and the remaining of quality B. This means that horizontal and vertical 68 per cent confidence interval is <1.34 km

for quality A and <2.67 km for quality B (Lahr 1999). More than 60 per cent of events have azimuthal gap less than 100°.

Repicking the seismic events also led to obtain a *P*-wave polarity data set that we used to compute focal mechanisms by means of the standard FPFIT grid-search algorithm (Reasenberg & Oppenheimer 1985). The number of polarity data used (≥15) and the good azimuthal coverage of the seismic stations at short epicentral distance (<80 km) led to stable solutions, with average errors on the maximum likelihood solutions <10° for strike, dip and rake (Table 2). Location parameters for each focal mechanisms are listed in Table 2.

3.2 Fault mapping and kinematic data analysis

We carried a detailed geological survey (scale 1:10.000) in the area struck by the 2013–2014 sequence. Predictably, we did not observe any evidence of surface coseismic effects, because of the limited energy and, as detailed in the Results section, the high nucleation depth of the main shock. Instead, field work was aimed at reconstructing the geometry and kinematics of recent normal faults. Particularly, fault-kinematic analysis allowed us to investigate the relation between the long-term strain field recorded by faults and the incremental strain field provided by focal mechanisms of the main shocks during the seismic sequence.

Fault-slip data were collected, following well-established criteria (e.g. Petit 1987), along the main fault surfaces or on footwall synthetic and antithetic faults in close proximity of the main fault. Care was taken in detecting consistent superposition relations between different striation sets on the same fault surface, which could reveal the existence of temporally discrete episodes of deformation under different stress fields. As detailed in the Results section, we consistently observed superposition of two sets of slip lineations, respectively assigned to two different stress regime stages. For each lineation set, we made a statistical analysis of the fault-slip data on individual faults by means of the inversion technique of Marrett & Allmendinger (1990) in order to compute the orientation of kinematic axes and determine the tectonic regime. For this inversion, we used ≥4, but usually more, slip orientations on non-parallel faults measured at individual sites (Table 3).

3.3 Geodetic data collection and processing

In order to ascertain the existence of an interseismic surface deformation pattern in the Matese Massif, all available GNSS data from both continuous and episodic measurements were collected, spanning ∼19 yr of observations from 1995.74 up to 2013.98. The data set includes 25 continuous GNSS sites (coming from various networks developed by national institutions and local agencies for geodynamic studies, mapping, engineering and cadastre purposes) located on a wide region encompassing the area of the seismic sequence, and two episodic GNSS sites belonging to the PTGA network (Ferranti *et al.* 2008, 2014).

Raw GNSS observations were processed using the GAMIT/GLOBK software packages (Herring *et al.* 2010) following the approach described in Palano (2015). To improve the overall configuration of the network and tie the regional measurements to an external global reference frame, data coming from 12 continuously operating global tracking stations (AJAC, BRUS, CAGL, GRAS, GRAZ, JOZE, LAMP, MATE, MEDI, NOTO, NOT1 and ZIMM), mostly from the EUREF (Beutler *et al.* 2008) permanent network, were introduced in the processing (see

Table 2. Hypocentral and kinematic parameters for focal mechanisms of events shown in Fig. 4, sorted by ascending date. ID: event; Date: yymmdd; Origin: origin time; Lat: latitude; Lon: longitude; Depth: depth of event (km); Mag: magnitude; Gap: maximum azimuthal gap between seismic stations; Dmin: minimum distance between epicentre and station; Rms: root mean square; Seh, Sez: semi-major principal axis of the 68 per cent joint-confidence ellipsoid for horizontal and vertical depth estimates, respectively; Str-A, Dip-A, Rak-A: strike, dip and rake, respectively, of plane A; Str-B, Dip-B, Rak-B: strike, dip and rake, respectively, of plane B; Az-*P*, Plg-*P*: azimuth and plunge, respectively, of *P*-axis; Az-*T*, Plg-*T*: azimuth and plunge, respectively, of *T*-axis.

ID	Date	Origin	Lat N	Lon E	Depth (km)	Mag	No	Gap (°)	Dmin (km)	Rms	Seh (km)	Sez (km)	Str-A (°)	Dip-A (°)	Rak-A (°)	Str-B (°)	Dip-B (°)	Rak-B (°)	Az-*P* (°)	Plg-*P* (°)	Az-*T* (°)	Plg-*T* (°)
0	131229	1703 25.14	41N22.15	14E26.39	17.64	2.7	27	44	5	0.36	0.1	0.2	95	50	–130	328	54	–53	298	60	32	2
1	131229	1708 43.35	41N22.70	14E26.41	17.86	4.9	33	43	5	0.46	0.1	0.1	120	50	–120	342	48	–59	322	67	230	1
2	131229	1726 47.45	41N21.87	14E26.48	15.78	2.9	29	44	6	0.33	0.1	0.2	85	55	–140	330	58	–42	295	51	27	2
3	131229	1729 45.05	41N22.49	14E25.27	14.85	3	28	46	4	0.37	0.1	0.2	105	45	–120	324	52	–63	295	69	35	3
4	131229	1811 54.06	41N23.45	14E25.33	16.57	2.8	27	41	4	0.45	0.7	0.3	105	50	–120	327	48	–59	307	67	215	8
5	131229	1949 49.47	41N21.51	14E26.78	14.76	3.7	28	45	6	0.49	0.2	0.2	20	50	–50	147	54	–127	356	60	263	2
6	131229	2135 35.30	41N23.91	14E25.06	16.62	2.9	31	43	4	0.35	0.3	0.6	110	45	–120	330	52	–63	300	69	40	4
7	131229	2203 27.43	41N23.52	14E24.85	14.08	3.2	29	42	3	0.33	0.2	0.3	315	35	–70	111	57	–103	344	74	210	11
8	131229	2231 32.93	41N24.33	14E26.03	16.87	2.8	37	41	5	0.58	0.1	0.8	110	45	–120	330	52	–63	301	69	320	3
9	131229	2334 01.37	41N24.23	14E26.16	15.79	3.1	37	41	5	0.46	0.3	0.2	125	50	–110	335	44	–67	330	74	229	3
10	131230	0128 16.86	41N21.32	14E27.77	13.31	2.4	37	58	8	0.49	0.1	0.2	60	40	–160	315	77	–52	262	44	16	22
11	131230	0355 13.35	41N21.48	14E27.29	14.81	2.4	29	48	7	0.33	0.2	0.3	105	25	–120	318	69	–77	249	64	37	22
12	131230	0412 06.45	41N22.73	14E27.65	17.8	3	35	38	7	0.33	0.1	0.1	15	45	–50	145	57	–122	0.5	62	257	6
13	140120	0712 40.08	41N22.06	14E27.28	17.38	4.2	42	39	7	0.48	0.2	0.1	335	65	–60	101	38	–137	287	59	43	14
14	140120	0721 16.48	41N22.21	14E28.08	17.33	2.7	26	56	8	0.54	0.1	0.2	100	35	–140	335	68	–61	283	57	44	18
15	140123	1127 07.75	41N20.29	14E28.23	14.25	2	23	52	5	0.32	0.1	0.2	115	45	–110	323	48	–71	302	76	39	2

Table 3. Fault kinematic measurements and resulting pseudo-focal mechanism parameters for tectonic events 1 and 2 on the specified fault, computed at each site from slip lineation inversion. Location shown in Fig. 4. Abbreviation on the structural position columns are: FWL, footwall lineations; MFL, main fault lineations; AL, all lineations. Fault label as in Fig. 3.

Site	Location	No. measures	Fault	Structural position	Nodal plane A		Nodal plane B		*P* axis		*T* axis	
					Trend (°)	Plunge (°)	Trend (°)	Plunge (°)	Trend (°)	Plunge (°)	Trend (°)	Plunge (°)
Event n. 1												
A	M. Crocetta	4	LF	FWL	109.2	37.6	336.6	62.5	290.1	62.5	47.6	13.5
B	Mutria NW	19	BSF	AL	124.9	51.3	299.9	38.8	54.2	83.3	212.6	6.2
C	Mutria S	5	BSF	FWL	137.3	19.8	268.9	76.6	160.2	56.1	10.8	30.1
D	Regia Piana	7	BSF	MFL	98.7	68.3	324.3	29.6	337.6	61.2	204.1	20.7
E	Rio Torbido	10	BSF	MFL	107.9	59.2	307.0	32.2	351.7	73.8	205.2	13.7
F	Civita Pietraroja	11	BSF	AL	120.0	68.3	297.8	21.2	31.4	66.2	209.4	23.8
G	Civita Cusano	5	BSF	MFL	117.6	51.0	306.8	39.3	353.8	82.6	211.8	5.9
H	M. Montorfano	10	SGF	MFL	92.0	57.6	302.5	36.4	320.0	71.5	194.5	11.0
I	Serrone	5	SGF	MFL	116.6	47.7	320.0	44.7	315.2	78.0	218.0	1.5
L	V. Paterno	11	CMF	AL	136.2	57.6	338.2	34.4	12.8	74.2	235.0	11.8
M	Cila-M. Stufo	12	PMF	AL	314.4	45.4	135.7	44.6	163.9	89.2	45.1	0.4
Event n. 2												
D	Regia Piana	7	BSF	MFL	90.9	62.3	227.3	36.0	42.2	64.3	163.7	14.1
E	Rio Torbido	5	BSF	MFL	60.8	69.9	266.5	31.7	301.2	71.0	160.4	14.9
H	M. Montorfano	6	SGF	MFL	55.3	74.9	196.9	19.0	341.2	58.5	135.9	29.0

Ferranti *et al.* 2014). In a following step, the GAMIT solutions were combined by means of GLOBK software package to estimate a consistent set of positions and velocities in a fixed Eurasian reference frame (Palano 2015).

4 RESULTS

4.1 Hypocentral distribution and focal mechanism solutions

The epicentral distribution of ∼250 best-located events of the sequence, whose local magnitude is $1.8 \leq M_L \leq 4.9$, is shown in Fig. 3a. The epicentral distribution depicts a ∼10 km long, NNW–SSE trending alignment within the southeastern sector of the Matese Massif (Fig. 3a), about 15 km southwest of the epicentral area of the 1997–1998 sequence (Fig. 2). The location of the first main shock ($M_L = 4.9$) falls slightly northwest of the middle of the sequence alignment, and the second main shock ($M_L = 4.2$) is shifted to the southeast relative to the first one (Fig. 3a).

The hypocentral distribution shows that the events are almost continuously distributed between 10 and 20 km depth (Figs 3b and c). However, two group of events can be distinguished. The deeper one is between 16 and 19 km, and includes the two main shocks (∼17–18 km), the foreshock, and a large number of $M_L > 2.8$ events. A shallower group of events is between 11 and 15 km, and shows a concentration around 14 km, which includes ∼30 per cent of the relocated events. A minor number of events occurred between 9 and 11 km depth. Very few events are located above 9 km and below 20 km. The hypocentral distribution in a cross-section orthogonal to the main regional structures outlines a narrow subvertical alignment (Fig. 3c). The distribution of the deeper (16–19 km) events gently dips toward the southwest.

The computed focal mechanisms show normal dip-slip features (Fig. 4; Table 2), in agreement with the analysis of D'Amico *et al.* (2014). The focal mechanism of the foreshock (n. 0 in Fig. 4), of the first main shock (n. 1), as well as those related to events with $M_L > 2.8$ show NW–SE striking planes. Instead, solutions n. 5 and 12 show ∼N–S striking planes. Focal mechanisms relative to the second main shock (n. 13 in Fig. 4) and the following events show NW–SE striking planes as well.

We applied the Gephart & Forsyth (1984) procedure to invert the focal mechanisms for the determination of the principal stress axes (σ_1, σ_2, σ_3) and the dimensionless parameter $R = \frac{(\sigma_2-\sigma_1)}{(\sigma_3-\sigma_1)}$ that describes the relative magnitudes of the principal stresses. The method identifies the best stress tensor model that most closely matches all the fault plane solutions of the source region. It requires the basic assumptions that the stress is uniform in space and time domains in the investigated volume. A variable misfit (F), given by the angular difference between the observed slip direction on a fault plane and the shear stress derived from the stress model, provides a guide to how well the assumption of stress homogeneity is fulfilled (Michael 1987). We performed an inversion using the whole focal mechanism data set. The result indicates a stress tensor with normal faulting regime features, where σ_1 axis is subvertical and σ_3 axis is subhorizontal and aligned along the NE–SW direction (Fig. 5).

4.2. Geometry and kinematics of upper crustal normal faults

The north–northwest-trending epicentral alignment runs in the internal part of the massif, and broadly parallels the trace of the eastern part of the MLF (Figs 2 and 4). Detailed geological-structural mapping has shown that the MLF is formed by discrete segments, which show an en-echelon arrangement and have individual length of the order of ∼10–15 km (Figs 3a and 4). Here we focus attention on the eastern segment (Bocca della Selva Fault - BSF), and to ancillary synthetic faults (San Gregorio and Castello Matese faults, SGF and CMF, Fig. 4), because of their proximity to the epicentral location of the seismic sequence.

Despite the fact that few exposures of the main fault surfaces were observed, results of fault-slip lineation analysis consistently show that the BSF and accompanying southwest-dipping faults have a primarily normal faulting behaviour. Based on the striation superposition relation, consistently observed on fault surfaces at several locales in the central and eastern part of the massif, two episodes of motion related to as many strain fields are observed (Fig. 4; Ferranti 1997). The first episode is relatively more significant, in

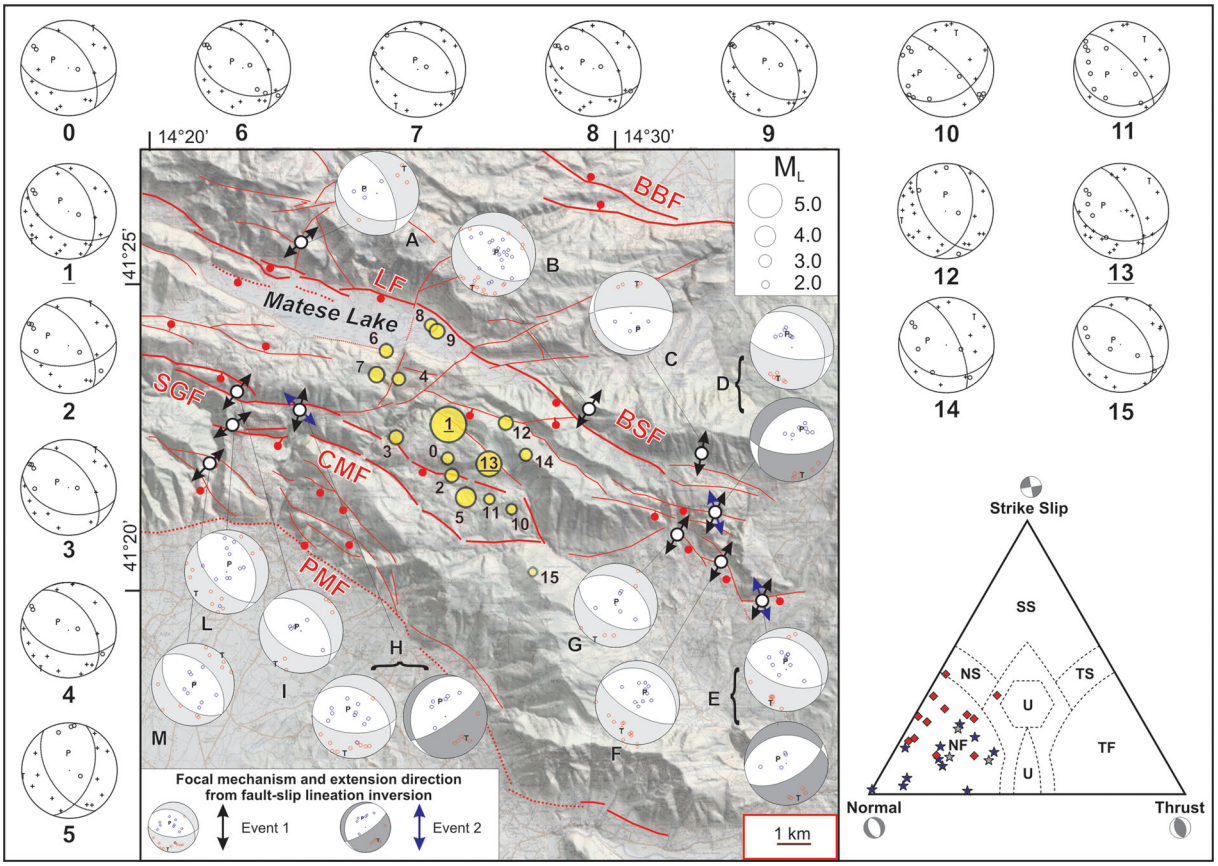

Figure 4. Fault-kinematic map of eastern Matese, and (outside map) computed focal mechanisms for the 2013–2014 sequence. Numbers under focal mechanisms refer to Table 2, underlined for the two main shocks (n. 1 and 13, respectively). Yellow circles are epicentres of computed focal mechanisms. Pseudo-focal mechanisms computed from slip lineation inversion are reported inside the map. Letters under pseudo-focal mechanisms refer to Table 3. Arrows are computed trends of finite extension axis for events n. 1 and 2 at each site. On the right bottom side, ternary plot of focal mechanisms (red diamonds) and pseudo-focal mechanisms (blue and grey stars for event n. 1 and 2, respectively) data is also reported. Each point is plotted based on the plunge of the P-, T- and B-axes of the mechanism (Frohlich 1992). Fault labels as in Fig. 3.

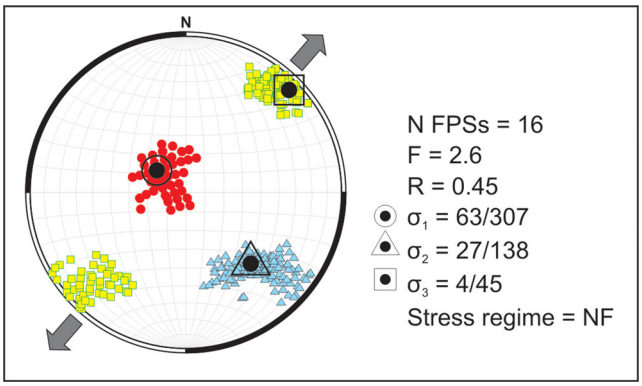

Figure 5. Results of the stress inversion (Gephart & Forsyth 1984) using focal mechanisms computed in this study (see Table 2 for details). *N* is the number of inverted earthquakes. Values *F* and *R* are explained in the text.

qualitative terms of duration/amount, as suggested by the morphology and development of slip indicators on fault surfaces. Inversion of slip lineations yields a tensile axis trending between NE–SW and NNE–SSW (Fig. 4, Table 3). The second slip episode, of relatively minor importance, has been observed at the southeast termination of the BSF, but also on the SGF, and is characterized by NW–SE to NNW–SSE trending computed tensile axes (Fig. 4, Table 3).

Few constraints exist on the age of extension. Faults recording both displacement stages cut middle-late Miocene marine carbonates and siliciclastic rocks, and locally undated continental scree deposits of probable early Pleistocene age.

4.3 Geodetic interseismic strain

To better detect a deformation signal over the investigated area, the GNSS velocities were referred to a local reference frame by subtracting from all sites the average velocity of ALIF and VAGA sites, located in the southern part of the massif (Fig. 6). Then, geodetic slip-rates were computed for both MLF and BBF (Table 4). Because of the low differential velocity and the sparse site coverage we adopted a simplified geometric model for the MLF (similar to the fault model used by Ferranti *et al.* 2014), which does not take into account individual segments such as the BSF (Fig. 6). More in details, we computed the parallel (strike) and perpendicular (tensile) horizontal components of the geodetic slip-rate by using a geometrical approach that projects the vector of GNSS site velocities onto the fault trace for both hanging-wall and footwall of the faults. Slip-rate components were estimated with a Monte Carlo simulation (Metropolis & Ulam 1949) by sampling the probability distributions of site velocities. The slip-rate estimations and their associated standard deviations were calculated from the estimated *a posteriori* probability distribution. Note that the geodetic slip-rate

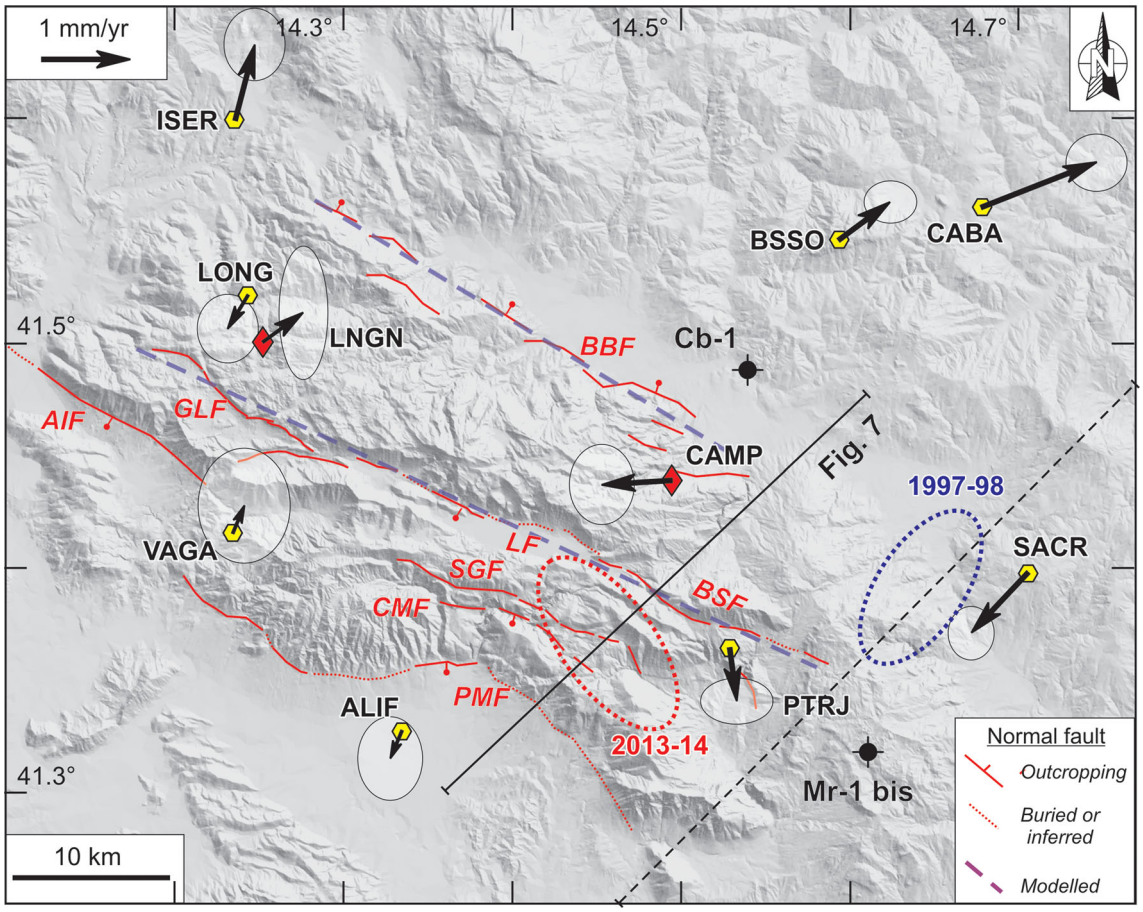

Figure 6. GNSS velocities in a local reference frame (see text for details). Error ellipses refer to 2σ (95 per cent) confidence level. Red solid or dotted lines represent outcropping or inferred/buried faults, and dashed blue lines are the simplified geometric model used for the geodetic slip-rate computation. GLF, Gallo-Letino fault; other fault labels as in previous figures. Red and blue ellipses are epicentral areas of the 2013–2014 and 1997–1998 sequences, respectively. Solid and dashed black lines are the traces of the crustal profile (Fig. 7) and of the tomographic image of Bisio *et al.* (2004), respectively.

estimation presented here for both faults is based on a longer time series relative to the previous estimate (e.g. Ferranti *et al.* 2014).

Slip-rates estimates evidence that the MLF is characterized by a statistically negligible geodetic motion (Table 4). This result might be taken to indicate that the fault is not linked to the deep seismogenic structure, or alternatively that it was locked before onset of the seismic sequence. We note, however, that all stations in both the hanging-wall and footwall except for PTRJ are located at a distance $\geq$5 km, which can be considered as a threshold for recording near-field effects for such a long fault (Savage & Burford 1973). This observation would point against interseismic strain accumulation on the fault. When we consider site PTRJ, which is the closest to the seismic sequence and is located near-fault (Fig. 6), a small left-oblique divergence is apparent, which could indeed point to an interseismic strain accumulation along a ~NNW–SSE trend consistent with that of the last kinematic episode recorded on the fault (Fig. 4).

Opposite to sites located around the MLF, sites straddled by the BBF show a marked divergence (Fig. 6). Geodetic analysis indicates significant extension (1.6 ± 0.4 mm yr^{-1}) in the far-field of the fault (Table 4), along a direction consistent with the seismological strain field of the Apennines. Our extension slip estimation is broadly consistent with the estimate of Giuliani *et al.* (2009) and Ferranti *et al.* (2014) and moderately larger than the inferred Pleistocene and Holocene rate for the fault proper (Galli & Galadini 2003).

5 DISCUSSION

5.1 Crustal model

Blending of geological and seismological data allows constructing the crustal structure which hosted the 2013–2014 sequence. To illustrate this, we draw a SW–NE trending crustal profile across both the seismic alignment and the extensional faults (Figs 6 and 7). The crustal structure was built using field, drillings and geophysical data for progressively deeper part of the profile, respectively. Specifically, we employed field observations and oil exploration well logs to model the thickness of the shallower tectonic units and the position and geometry of tectonic horizons. Deeper horizons were traced from extrapolation of regional stratigraphy and structural data calibrated against the seismic tomography results of Bisio *et al.* (2004). We draw our geological profile parallel and ~10 km to the northwest of tomographic profile B–B′ of Bisio *et al.* (2004). Our profile is within the well-resolved area of the tomographic image (dashed grey line in Fig. 7).

The uppermost tectonic horizon in the model is represented by the thrust surface carrying the Matese platform carbonates above the Molisan basin rocks (Fig. 7). Attitude and depth of this surface are extrapolated from the thickness (~3.5–4 km) of the Matese platform succession known from surface observations (e.g. D'Argenio *et al.* 1973) and from well logs (Campobasso 1 and Frosolone 2 wells, Table 5; Calabrò *et al.* 2003). Wells north and east of Matese

Table 4. Model parameters and geodetic slip-rate for the Matese Lake and Boiano Basin faults.

Fault segment name	Length (km)	Coordinate		Down-dip width (km)	Min depth (km)	Max depth (km)	Strike/dip/rake (°)	Kinematic geology	Dip direction	GPS sites		Geodetic slip-rate (mm yr^{-1})	
		West tip	East tip							Footwall	Hangingwall	Strike-slip (mm)	Opening (mm)
Matese Lake	36	41°30′22″ 14°8′47″	41°21′33″ 14°32′19″	14.3	0	13–17	116/65/270	N	SW	LNGN, LONG, CAMP	VAGA, ALIF, PTRJ	0.27 ± 0.50	0.03 ± 0.65
Boiano Basin	24	41°31′22″ 14°19′5″	41°24′5″ 14°33′56″	13.8	1	12.3	120/55/270	N	NE	LONG, CAMP	BSSO, CABA	0.23 ± 0.41	1.58 ± 0.41

document that, at places, the Matese platform rocks are structurally interleaved between different imbricates of Molisan units (Campobasso 1 and Morcone 1bis wells, Table 5; Fig. 7), as a consequence of a triangle zone developed in the frontal zone of the thrust sheet. In contrast, beneath the Matese massif, the Molisan basinal rocks are extensively overthrust by the platform rocks, but the precise thickness of the Molisan thrust sheet is difficult to establish because it is typically composed of an unknown number of relatively thin imbricates (Di Bucci *et al.* 2005a). In deep wells around the Matese area, the Molisan thrust assemblage thrust above the Apulia platform has a compound thickness ranging from 2 to 4 km, which also includes a basal tectonic mélange (Table 5). We thus adopted a laterally variable thickness, which places the basal thrust of the Molisan unit above the Apulia platform at a variable depth of ∼6–8 km moving from north to south. The depth of this horizon has been calibrated to broadly fit, in the tomographic image of Bisio *et al.* (2004), a *P*-wave velocity of ∼6 km s^{-1} (Fig. 7).

The thickness of the Apulia carbonate platform as recorded by deep wells in the foreland is ∼6–7 km (Improta *et al.* 2010), and Apulian carbonate rocks underlying the Matese Apennines are likely to have a similar thickness. Thus, the base of the Apulia sedimentary succession is placed in our model at a depth variable from 13 to 15 km moving from northern to southern Matese, respectively (Fig. 7). *P*-wave velocities in this unit increase from ∼6.0 to ∼6.6 km s^{-1}, consistent with values typically assigned to the Apulia carbonate and evaporite rocks (Improta *et al.* 2002). The subjacent crust is formed by the pre-Mesozoic Apulia crystalline basement and overlying epiclastic deposits, with *P*-velocities > 6.6 km s^{-1}.

Within the tomographic image of Bisio *et al.* (2004), the deep *P*-velocity isochrones (≥6.0 km s^{-1}), which are those assigned to the Apulia unit, form structural highs and lows that arguably result from the late Pliocene–early Pleistocene shortening events of the Apennines orogeny (Bisio *et al.* 2004; Di Bucci *et al.* 2005a). Oblique thrusts and transpressional faults, locally mapped at surface (Ferranti 1997) may mark the differential uplift of distinct Apulian blocks. This interpretation is supported by a wealth of oil exploration data in the Apennines (Di Bucci *et al.* 2005a; Nicolai & Gambini 2007).

The mapped southwest-dipping normal faults are traced through the Matese and the Molisan thrust sheets, as observed in surface exposures and in interpreted seismic profiles (Casero *et al.* 1988). However, based on regional analogues (e.g. Di Bucci *et al.* 2005a,b), most of these faults may cut through at least the Apulia sedimentary crust, where they should progressively flatten downdip (dotted in Fig. 7). Although regional field relations indicate that the extensional faults were superposed onto the compressive and transpressive structures after the early Pleistocene (Ferranti 1997; Di Bucci *et al.* 2005a,b), we argue that they have caused only a minor displacement of the previous structural fabrics. This inference is based on the downward projection of the offset measured in the field across the extensional faults, and indicated for the base of the Matese thrust sheet in Fig. 7. The offset does not match the underlying broad bulge of the Apulia unit, supporting the contention that the bulge results from earlier shortening.

We do not exclude that some of the normal faults started moving during the late Pliocene–early Pleistocene and developed in response to deep contractional and transpressional uplift. The fact that a second extension stage with ∼NNW–SSE trending tensile axis is recorded on these faults suggests actually that the older, main stage, with ∼NE–SW tensile axis, akin to the seismologically determined tensile axis in the Apennines (Montone *et al.* 2012), may be indeed a relic of an older deformation.

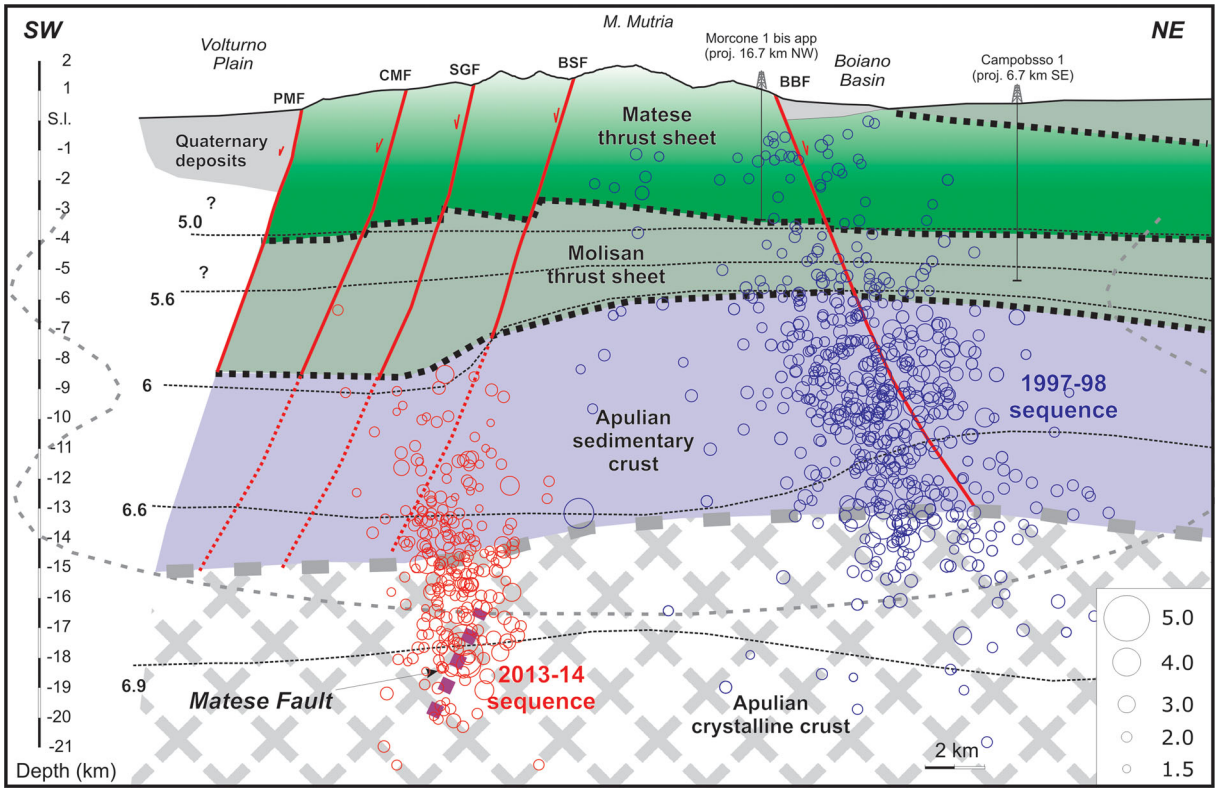

Figure 7. Crustal structure underneath eastern Matese with projected hypocentres of the 2013–2014 (red dots) and 1997–1998 (blue dots) seismic sequences. Thick dotted black lines are main tectonic horizons. Thick dashed grey line is inferred transition between crystalline and sedimentary rocks of Apulian. Thin dotted black lines and thin dashed grey line are velocity isochrones and the well-resolved part, respectively of the seismic tomography image (Bisio *et al.* 2004).

Table 5. Well log data used in this study (see Fig. 2 for location).

Well	Longitude E	Latitude N	Ground level (m a.s.l.)	Tectonic unit	Depth interval (m)	N. imbricates	Total thickness (m)
Campobasso 1	02°05′28″	41°29′04″	477	Sannio-Molisan	0–800	1	800
				Matese (flysch)	800–1832	1	1032
				Matese (carbonate)	1832–5436	2	3604
				Sannio-Molisan	5436–5860	1	424
Frosolone 2	01°56′04″	41°36′58″	1300	Matese (carbonate)	0–3540	2	3540
				Sannio-Molisan	3540–3993	1	453
Mirabello 1	02°14′18″	41°29′11″	750	Sannio-Molisan	0–4212	2	4212
Moilinara Nord 1	02°28′31″	41°19′54″	724	Sannio-Molisan	0–4032	2	4032
				Apulia	4032–5400	1	1368
M. Taburno 1	02°15′33″	41°07′20″	210	Sannio-Molisan	0–2094	4	2094
				Apulia	2094–3733	1	1639
Morcone 1 bis	02°09′44″	41°18′54″	984	Sannio-Molisan	0–545	2	545
				Matese (flysch)	545–1325	1	780
				Matese (carbonate)	1325–4198	1	2873

Specifically, the older stage of extension may be contemporaneous to deep transpression, and does not relate to the current seismogenic regime.

On the northeastern border of Matese, the northeast-dipping BBF is shown to cut through the upper thrust sheet and the Apulia sedimentary section (Fig. 7). The fault has been active since the middle Pleistocene (Di Bucci *et al.* 2005b) and has a kinematic compatible with the present geodetic and seismic strain fields (Fig. 5).

Intriguing relations between crustal structure and seismogenesis emerge when the hypocentres of the 2013–2014 and 1997–1998 sequences are plotted on the constructed crustal model (Fig. 7). Whereas the profile crosses in the middle the 2013–2014 sequence, the 1997–1998 sequence is projected ∼10 km to the northwest (Fig. 6). The width of the 1997–1998 sequence projected onto the profile is quite narrow (∼5 km), and we assume no strong variation in the crustal structure of the volume hosting the two sequences.

As concern the 2013–2014 sequence, the focal volume containing the foreshock, the two main shocks, and many $M_L > 2.8$ events is confined within the crystalline crust of Apulia below 16 km of depth. The above hypocentres allow proposing a depth for the causative fault of the seismic sequence, here named Matese fault, between 16 and 20 km. Events between 11 and 15 km occurred within the Apulia sedimentary cover, and are characterized by a concentration

at ∼14 km (Fig. 7). Basically, seismicity stopped within the Apulia unit and did not interest the overlying Molisan and Matese rootless thrust sheets.

Instead, almost all events of the 1997–1998 sequence are continuously distributed between 5 and 15 km depth. The sequence main shock (duration magnitude $M_D = 4.2$) as well as almost all $M_D > 3.0$ events had a focal depth at ∼13–14 km, coincident with the proposed rooting depth of the BBF (DISS Working Group 2010) and with our inferred depth for the crust-sedimentary transition in northern Matese (Fig. 7).

5.2 The Matese seismogenic structure

Seismological and geological arguments suggest that the Matese fault is a SW-dipping structure. We regard the SW-dipping nodal plane of the main shocks as the rupture surface for the following lines of reasoning. First, according to felt reports (http://www.haisentitoilterremoto.it/repository/7231389480/index.html), the largest MCS intensities of up to VII are located in the Volturno basin which flanks the massif to the SW (Fig. 3; Convertito *et al.* 2014). Although the macroseismic field is certainly in part influenced by site effects, we stress that far (∼80 km) localities to the southwest, such as Naples and the Tyrrhenian coast (Fig. 1), felt the earthquakes more largely (up to IV) than equally distant regions to the northeast of the massif.

Second, a southwest-dipping deep seismogenic structure would be in accordance with the geometry of mapped crustal faults all of which, in southern Matese, have the same dip direction (Fig. 7). The upward projection of the seismic alignment intersects the earth surface very close to the BSF (Fig. 7). Although, as discussed above, this latter and the ancillary faults may be inherited structures from an older deformation stage, the possibility that they are occasionally activated during infrequent earthquakes should not be discarded. However, resolving to what degree the deep causative fault in the Apulia crystalline crust and the upper crustal faults are linked is not a simple task. To this end, a reconstruction of the evolution of the 2013–2014 sequence offers vital insights.

According to well-established empirical relations between earthquake magnitude and fault size (Wells & Coppersmith 1994), only a limited-length (∼1 km) segment of the Matese fault failed during the first main shock, and, as discussed above, the rupture did not propagate across the inferred contact between crystalline and sedimentary Apulian rocks at ∼15 km depth. The second main shock and additional $M_L > 2.8$ events continued rupturing a ∼10 km long section of the deep fault. Part of the ensuing seismic sequence activated a comparably long section of an overlying extensional fault between 11 and 15 km depth (Figs 3b and 7). Although it cannot be unquestionably proven, it is possible that this fault corresponds to the deep part of the BSF, which is located straight upon the shallower seismic alignment. Effectively, the alignment stops to the north at the en-echelon boundary between the LF and the BSF. To the south, the alignment vanishes parallel to the splay termination of the BSF (Figs 3a and 4).

We argue that activation of the deep part of the BSF during the 2013–2014 seismic sequence occurred passively, possibly through pore fluid pressure diffusion (e.g. Malagnini *et al.* 2012). A passive activation of the BSF is suggested by the uneven distribution of the events in the seismic alignment (Fig. 6). The deep discontinuity at 15 km, albeit limiting upward the coseismic rupture propagation, did not halt diffusion of the pressurized fluids released during the fault-valve action (Sibson 1992) of the main shocks, implying hydraulic connection between the Matese fault and the deep section of the BSF.

As argued above, the southwest-dipping upper crustal faults possibly developed during the Pliocene–early Pleistocene tectonics, and during mid-Pleistocene to contemporary extension they played only a minor role. The last kinematic episode recorded by slip lineation on these faults, which is characterized by NNW–SSE extension and is chiefly observed at the SE termination of the array (Fig. 4), is consistent with the extension axis computed for the 1997–1998 sequence main shocks, which occurred at the SE boundary of the BBF (Fig. 2; Milano *et al.* 2002). Additionally, a minor NNW–SSE trending tensile strain accumulation on the BSF, almost orthogonal to the seismically released strain during the 2013–2014 sequence, is possibly reflected in the geodetic velocity residuals (Fig. 6). These observations concur to underscore that the shallow crustal faults may be locally activated today, but they are unlikely to be important seismogenic sources. Conversely, the deep Matese fault, which might be an inherited structure from the late Permian to early Cretaceous rifting that affected the Apulia and the whole Adriatic plate (Fantoni & Franciosi 2010), is nowadays focusing the seismic deformation in the middle crust underneath Matese.

However, we cannot definitely exclude that deep and shallow structures may be occasionally linked to form a single focal volume. The BSF and ancillary faults to the SW do not show clear surface evidence of ancient coseismic events: this observation, together with our slip lineation and geodetic analysis suggests that, even if linked, surface ruptures during large earthquakes are unlikely. Indeed, the position of the seismic sequence in between sources of destructive historical earthquakes, namely the 1349 and 1688 events (Fig. 2), is of some concern. This also because the 1349 event, which occurred to the west of the high Apennines extensional belt, together with the 2013–2014 sequence, may be evidence of the seismogenic potential of southwest-dipping extensional faults.

5.3 Regional seismotectonic implications

The Matese seismic sequence represents an anomaly in the established seismotectonic pattern of the Southern Apennines extensional belt, because of the remarkable depth (17–18 km) of the main shocks. The $M_w = 6.9$, 1980 earthquake, which was caused by normal displacement on the northeast-dipping Irpinia fault in the southern array of the regional extension belt (Fig. 1) had a focal depth of 13.7 km (Pondrelli *et al.* 2006), and an equivalent seismogenic depth is typically attributed to the extensional faults of the Apennines (Chiarabba *et al.* 2005; DISS Working Group 2010; Ferranti *et al.* 2014). East of the high mountains, moderate strike-slip earthquakes with a focal depth comparable to the 2013–2014 Matese sequence, occur on ∼E–W striking right-lateral faults, such as the 2002 San Giuliano di Puglia earthquake sequence which occurred ∼50 km northeast of Matese (Figs 1 and 2; Di Luccio *et al.* 2005). Other ∼E–W trending seismogenic sources are inferred for large historical earthquakes east of the Apennines (Fig. 2; Fracassi & Valensise 2007; DISS Working Group 2010).

The Matese fault differs from both the Irpinia-type and the San Giuliano-type seismogenic faults, because it is relatively deep, has a southwestern dip, and an extensional kinematics. We argue that the Matese fault represents a third, and so far little investigated seismogenic structure in the Southern Apennines. We speculate that the source of the 1349 earthquake, which had a wide-ranging macroseismic field (Galli & Naso 2009), as well as other unknown

faults relatable to ancient earthquakes (e.g. 1688) are somewhat similar to the Matese fault.

On the contrary, the BBF, located at the northeastern border of the Matese Massif, and considered responsible for the $M_w = 6.6$, 1805 earthquake (Fig. 2), is akin to the Irpinia-type model insofar it has a northeast dip and a kinematic consistent with the present extensional regime (Di Bucci *et al.* 2005b). Furthermore, unlike the Matese fault and overlying upper crustal faults, the BBF has a significant geodetic interseismic strain accumulation along a ∼NE–SW direction (Fig. 6, Table 4; Giuliani *et al.* 2009; Ferranti *et al.* 2014). Noteworthy, the 1997–1998 and 2001 sequences, which are located at the southeast and northwest tip of the BBF, respectively (Fig. 2), and presumably mark its lateral boundaries, chiefly occurred within the first ∼15 km of the crust (Fig. 7; Milano *et al.* 2002, 2005). This occurrence supports the attribution of the BBF to the Irpinia-type model.

The question arises then why the Boiano Basin and the Matese faults have so different features within a so close stretch of crust. To this end, the inherited crustal structure provides an insightful clue. Inspection of tomographic images (Bisio *et al.* 2004) and of a fragmentary reconstruction of the architecture of the Apulia platform provided by oil exploration data (Nicolai & Gambini 2007), indicate that the late Pliocene–early Pleistocene compressive structure underlying the Matese Massif culminates north of the BSF and of the 2013–2014 seismic sequence (Fig. 7). Because the cold and thick Apulia platform and underlying crystalline basement represent the crustal layer where extensional seismogenesis occurs in the Apennines (Chiarabba & Amato 1996; Bisio *et al.* 2004), the different position of this assemblage in northern and southern Matese may control the close concurrence of both the Irpinia-type and Matese-type seismogenic structures.

It is possible that Matese-type structures characterize other sections of the northern array of the Apennines active extensional belt and perhaps of the southern array as well (Fig. 1). If so, moderate or large earthquakes on these structures would be infrequent but widely-felt, because of the deeper position of Apulian imbricates on the southwest flank of the high Apennines (Nicolai & Gambini 2007). This could explain the meager recognition of SW-dipping seismogenic structures in the active fault record and in the instrumental and historical seismicity catalogues.

6 CONCLUSIONS

The 2013–2014 seismic sequence in southern Matese is another good example of the role played by the inherited structural grain on the present day Italian seismic release, in terms of controlling downdip and along-strike segmentation of the seismogenic faults, and the slip distribution at depth during earthquakes. This has been recently highlighted by the M_w 6.3, 2009 L'Aquila and M_w 6.1, 2012 Emilia seismic sequences, during which the geometry of the fault rupture and the aftershock distribution were mostly controlled by the presence of inherited tectonic discontinuities (Bigi *et al.* 2012; Bonini *et al.* 2014a,b).

The Matese sequence was initiated by slip on a deep (16–20 km) SW-dipping extensional fault (the Matese fault). The main coseismic ruptures occurred within the Apulia crystalline crust, likely along an inherited discontinuity, and stopped at the ∼15 km deep transition with the overlaying sedimentary crust. A shallower group of events within the Apulia sedimentary crust (∼11–15 km) may be evidence of passive reactivation of pre-existing southwest-dipping normal faults, and specifically the BSF.

These uppermost crustal normal faults possibly formed during late Pliocene–early Pleistocene transpressional uplift of Apulia imbricates at depth, but they play a minor role in the current seismogenic regime. In fact, they have poor expression of past coseismic activity, have a last kinematic of NNW–SSE extension different from the NE–SW extension recorded by the seismic sequence under study, and show little or no geodetic interseismic strain accumulation.

On the contrary, the northeast-dipping BBF, located in northern Matese adjacent to the area of the 2013–2014 sequence, offers clear evidence of pre-historical to recent activity, and is characterized by a ∼NE–SW trending extension axis and by a significant co-axial geodetic strain.

We relate the dissimilar behaviour of the Matese and the Boiano Basin faults, which are very close in space, to the different crustal architecture inherited from previous shortening events. A larger transpressive uplift of the cold Apulia sedimentary and crystalline crust, where extensional seismogenesis typically occurs in the Apennines, is observed in northern relative to southern Matese. This could have enhanced, on the northeast side of the massif, the easier growth of shallower normal faults with more frequent earthquakes and with geodetic evidence of interseismic strain accumulation.

However, we do not exclude that the Matese fault and the shallower SW-dipping faults could be linked during infrequent earthquakes, albeit the deeper position of the seismogenic structure, when compared to the Irpinia or Boiano faults, makes unlikely a propagation to the surface of the rupture. The location of the Matese fault in between sources of destructive historical earthquakes must be regarded with caution, and this occurrence could characterize also other sections of the Southern Apennines extensional belt.

ACKNOWLEDGEMENTS

We thank Dario Slejko and an anonymous reviewer for their critical reviews and constructive comments that improved the paper. We appreciated the suggestions and useful comments by Editor Prof. Egill Hauksson. We are grateful to all individuals and institutions for contributing the GNSS data, particularly to the technical staff of INGV who continue to maintain the RING network. We are grateful to Leica Geosystems S.P.A. (http://it.smartnet-eu.com) and Regione Campania (http://gps.sit.regione.campania.it/indexmain.php) for providing free access to GNSS data.

REFERENCES

Beutler, G., Moore, A.W. & Mueller, I.I., 2008. The International Global Navigation Satellite Systems (GNSS) Service: developments and achievements, *J. Geod.,* **83**(3–4), 297–307.

Bigi, S., Casero, P., Chiarabba, C. & Di Bucci, D., 2012. Contrasting surface active faults and deep seismogenic sources unveiled by the 2009 L'Aquila earthquake sequence (Italy), *Terra Nova,* **25**(1), 21–29.

Bisio, L., Di Giovambattista, R., Milano, G. & Chiarabba, C., 2004. Three-dimensional earthquake locations and upper crustal structure of the Sannio- Matese region (Southern Italy), *Tectonophysics,* **385,** 121–136.

Bonini, L., Di Bucci, D., Toscani, G., Seno, S. & Valensise, G., 2014a. On the complexity of surface ruptures during normal faulting earthquakes: excerpts from the 6 April 2009 L'Aquila (central Italy) earthquake (Mw 6.3), *J. geophys. Res.: Solid Earth,* **5,** 389–408.

Bonini, L., Toscani, G. & Seno, S., 2014b. Three-dimensional segmentation and different rupture behavior during the 2012 Emilia seismic sequence (Northern Italy), *Tectonophysics,* **630,** 33–42.

Bousquet, J.C., Grellet, B. & Sauret, B., 1993. Neotectonic setting of the Benevento area: comparison with the epicentral zone of the Irpinia earthquake, *Ann. Geofis.,* **36**(1), 245–251.

Calabrò, R.A., Corrado, S., Di Bucci, D., Robustini, P. & Tornaghi, M., 2003. Thin-skinned vs. thick-skinned tectonics in the Matese Masif, Central-Southern Apennines (Italy), *Tectonophysics,* **377,** 269–297.

Casero, P., Roure, F., Moretti, I., Muller, C., Sage, L. & Vially, R., 1988. Evoluzione geodinamica neogenica dell'Appennino Meridionale, *Mem. Soc. Geol. Ital.,* **41,** 109–119.

Chiarabba, C. & Amato, A., 1996. Crustal velocity structure of the Apennines (Italy) from *P*-wave travel time tomography, *Ann. Geofis.,* **39**(6), 1133–1148.

Chiarabba, C. & Frepoli, A., 1997. Minimum 1D velocity models in Central and Southern Italy: a contribution to better constrain hypocentral determinations, *Ann. Geofis.,* **40**(4), 937–954.

Chiarabba, C., Jovane, L. & Di Stefano, R., 2005. A new view of Italian seismicity using 20 years of instrumental recordings, *Tectonophysics,* **395,** 251–268.

Convertito, V., Cubellis, E., Maturano, A., Obrizzo, F. & Petrazzuoli, S.M., 2014. Terremoto del 29 Dicembre 2013 nel Matese ($M_W = 5.0$): indagine speditivi degli effetti nell'area epicentrale e analisi preliminare della sequenza sismica, Rapporti Tecnici INGV, 290, Available at: http://istituto.ingv.it/l-ingv/produzione-scientifica/rapporti-tecnici-ingv/.

D'Agostino, N., 2014. Complete seismic release of tectonic strain and earthquake recurrence in the Apennines (Italy), *Geophys. Res. Lett.,* **41,** 1155–1162.

D'Amico, S., Cammarata, L., Cangemi, M., Cavallaro, D. & DiMartino, R.M. & FirettoCarlino, M., 2014. Seismic moment tensors and regional stress in the area of the December 2013–January 2014, Matese earthquake sequence (Italy), *J. Geodyn.,* **82,** 118–124.

D'Argenio, B., Pescatore, T. & Scandone, P., 1973. Schema geologico dell'Appennino meridionale (Campania e Lucania): Convegno 'Moderne vedute sulla geologia dell'Apennino, *Atti Accademia Lincei,* **183,** 49–72.

De Gori, P. *et al.*, 2014. Le attività di pronto intervento sismico dell'INGV a seguito del terremoto del 29 Dicembre 2013, Rapporti Tecnici INGV, 281, Available at: http://istituto.ingv.it/l-ingv/produzione-scientifica/rapporti-tecnici-ingv/.

Di Bucci, D., Massa, B., Tornaghi, M. & Zuppetta, A., 2005a. Structural setting of the 1688 Sannio earthquake epicentral area (Southern Italy) from surface and subsurface data, *J. Geodyn.,* **40,** 294–315.

Di Bucci, D., Naso, G., Corrado, S. & Villa, I.M., 2005b. Growth, interaction and seismogenic potential of coupled active normal faults (Isernia Basin, central-southern Italy), *Terra Nova,* **17,** 44–55.

Di Luccio, F., Fukuyama, E. & Pino, N.A., 2005. The 2002 Molise earthquake sequence: what can we learn about the tectonics of southern Italy, *Tectonophysics,* **405**(1–4), 141–154.

DISS Working Group, 2010. Database of Individual Seismogenic Sources (DISS), Version 3.1.1: a compilation of potential sources for earthquakes larger than M 5.5 in Italy and surrounding areas, http://diss.rm.ingv.it/diss/, Ist. Naz. Geofis. Vulcanol, doi: 10.6092/INGV.IT-DISS3.1.1.

Doglioni, C., Harabaglia, P., Martinelli, G., Mongelli, F. & Zito, G., 1996. A geodynamic model of the Southern Apennines accretionary prism, *Terra Nova,* **8,** 540–547.

Fantoni, R. & Franciosi, R., 2010. Tectono-sedimentary setting of the Po Plain and Adriatic foreland, *Rend. Lincei,* **21**(1), S197–S209.

Ferranti, L., 1997. Tettonica tardo Pliocenica-Quaternari dei Monti del Matese (Appennino Meridionale): raccorciamenti tardivi e distensione "neotettonica", *Il Quaternario,* **10**(2), 501–504.

Ferranti, L. & Oldow, J.S., 2005. Latest Miocene to quaternary horizontal and vertical displacement rates during simultaneous contraction and extension in the Southern Apennines orogen, Italy, *Terra Nova,* **17,** 209–214.

Ferranti, L. *et al.*, 2008. Active deformation in Southern Italy, Sicily and southern Sardinia from GPS velocities of the Peri-Tyrrhenian Geodetic Array (PTGA), *Boll. Soc. Geol. Ital.,* **127**(2), 299–316.

Ferranti, L., Palano, M., Cannavò, F., Mazzella, M.E., Oldow, J.S., Gueguen, E., Mattia, M. & Monaco, C., 2014. Rates of geodetic deformation across active faults in southern Italy, *Tectonophysics,* **621,** 101–122.

Fracassi, U. & Milano, G., 2014. A soft linkage betweenmajor seismogenic fault systems in the central-southern Apennines (Italy): evidence from low-magnitude seismicity, *Tectonophysics,* **636,** 18–31.

Fracassi, U. & Valensise, G., 2007. Unveiling the sources of the catastrophic 1456 multiple earthquake: hints to an unexplored tectonic mechanism in Southern Italy, *Bull. seism. Soc. Am.,* **97**(3), 725–748.

Frohlich, C., 1992. Triangle diagrams: ternary graphs to display similarity and diversity of earthquake focal mechanisms, *Phys. Earth planet. Inter.,* **75,** 193–198.

Galadini, F., Meletti, C. & Rebez, A. (eds), 2000. *Le ricerche del GNDT nel campo della pericolosità sismica (1996–1999),* CNR-Gruppo Nazionale per la Difesa dai Terremoti.

Galli, P. & Galadini, F., 2003. Disruptive earthquakes revealed by faulted archaeological relics in Samnium (Molise, southern Italy), *Geophys. Res. Lett.,* **30,** 1266, doi: 10.1029/2002GL016456.

Galli, P.A.C. & Naso, J.A., 2009. Unmasking the 1349 earthquake source (southern Italy): palaeoseismological and archaeoseismological indications from the Aquae Iuliae fault, *J. Struct. Geol.,* **31,** 128–149.

Gephart, J.W. & Forsyth, W.D., 1984. An improved method for determining the regional stress tensor using earthquake focal mechanism data: applications to the San Fernando earthquake sequence, *J. geophys. Res.,* **89,** 9305–9320.

Giuliani, R., D'Agostino, N., D'Anastasio, E., Mattone, M., Bonci, L., Calcaterra, S., Gambino, P. & Merli, K., 2009. Active crustal extension and strain accumulation from GPS data in the Molise region (central-southern Apennines, Italy), *Boll. Geofis. Teor. Appl.,* **50**(2), 145–156.

Herring, T.A., King, R.W. & McClusky, S.C., 2010. *Introduction to GAMIT/GLOBK,* Release 10.4. Massachusetts Institute of Technology, Cambridge MA, pp. 1–48.

Hyppolite, J.C., Angelier, J. & Roure, F., 1994. A major geodynamic change revealed by quaternary stress patterns in the Southern Apennines (Italy), *Tectonophysics,* **230,** 199–210.

Iannaccone, G. *et al.*, 1998. A *P*-wave velocity model of upper crust of Sannio region (Southern Apennines), *Ann. Geofis.,* **41**(4), 567–582.

Improta, L., Iannaccone, G., Capuano, P., Zollo, A. & Scandone, P., 2002. Inference on the upper crustal structure of southern Apennines (Italy) from seismic refraction investigations and subsurface data, *Tectonophysics,* **317,** 273–297.

Improta, L. *et al.*, 2010. Detecting young, slow-slipping active faults by geologic and multidisciplinary high-resolution geophysical investigations: a case study from the Apennine seismic belt, Italy, *J. geophys. Res.,* **115,** B11307.

Lahr, J.C., 1999. HYPOELLIPSE: a computer program for determining local earthquake hypocentral parameters, magnitude, and first-motion pattern (Y2K compliant version), 1999 version 1.0, U.S. Geol. Sur., Open-File Report 99–23, 99 pp.

Lee, W.H.K. & Lahr, J.C., 1975. HYPO71 (revised): a computer program for determining hypocenter, magnitude and first motion pattern of local earthquakes, U.S. Geol. Sur., Open file Report, pp. 75–311.

Malagnini, L., Lucente, P., De Gori, P., Akinci, A. & Munafò, I., 2012. Control of pore fluid pressure diffusion on fault failure mode: insights from the 2009 L'Aquila seismic sequence, *J. geophys. Res.,* **117,** B05302, doi:10.1029/2011JB008911.

Marrett, R. & Allmendinger, R.W., 1990. Kinematic analysis of fault-slip data, *J. Struct. Geol.,* **12,** 973–986.

Maschio, L., Ferranti, L. & Burrato, P., 2005. Active extension in Val d'Agri area, Southern Apennines, Italy: implications for the geometry of the seismogenic belt, *Geophys. J. Int.,* **162,** 591–609.

Metropolis, N. & Ulam, S., 1949. The Monte Carlo method, *J. Am. Stat. Ass.,* **44**(247), 335–341.

Michael, A.J., 1987. Use of focal mechanisms to determine stress: a control study, *J. geophys. Res.,* **92,** 357–368.

Milano, G., Di Giovambattista, R. & Alessio, G., 1999. Earthquake swarms in the Southern Apennines chain (Italy): the 1997 seismic sequence in the Sannio-Matese mountains, *Tectonophysics,* **306**(1), 57–78.

Milano, G., Ventura, G. & Di Giovambattista, R., 2002. Seismic evidence of longitudinal extension in the Southern Apennines chain (Italy): the 1997–1998 Sannio-Matese seismic sequence, *Geophys. Res. Lett.,* **29**(20), doi: 10.1029/2002GL015188.

Milano, G., Di Giovambattista, R. & Ventura, G., 2008. Seismic activity in the transition zone between Southern and Central Apennines (Italy): evidences of longitudinal extension inside the Ortona-Roccamonfina tectonic line, *Tectonophysics,* **457**(1–2), 102–110.

Milano, G., Di Giovambattista, R. & Ventura, G., 2005. The 2001 seismic activity near Isernia (Italy): implications for the seismotectonics of the Central–Southern Apennines, *Tectonophysics,* **401**(3–4), 167–178.

Montone, P., Mariucci, M.M. & Pierdominici, S., 2012. The Italian present-day stress map, *Geophys. J. Int.,* **189,** 705–716.

Mostardini, F. & Merlini, S., 1986. Appennino centro-meridionale. Sezioni Geologiche e Proposta di Modello Strutturale, *Mem. Soc. Geol. Ital.,* **35,** 177–202.

Nicolai, C. & Gambini, R., 2007. Structural architecture of the Adria platform-and-basin system, *Boll. Soc. Geol. Ital.,* **7,** 21–37.

Palano, M., 2015. On the present-day crustal stress, strain-rate fields and mantle anisotropy pattern of Italy, *Geophys. J. Int.,* **200**(2), 969–985.

Palano, M., Cannavò, F., Ferranti, L., Mattia, M. & Mazzella, E., 2011. Strain and stress fields in the Southern Apennines (Italy) constrained by geodetic, seismological and borehole data, *Geophys. J. Int.,* **187**(3), 1270–1282.

Pantosti, D. & Valensise, G., 1990. Faulting mechanism and complexity of the November 23, 1980, Campania-Lucania Earthquake, inferred from surface observations, *J. geophys. Res.,* **95**(B10), 15 319–15 341.

Papanikolaou, I.D. & Roberts, G.P., 2007. Geometry, kinematics and deformation rates along the active normal fault system in the southern Apennines: implication for fault growth, *J. Struct. Geol.,* **29,** 166–188.

Patacca, E. & Scandone, P., 2007. Geological interpretation of the CROP-04 seismic line (southern Apennines, Italy), *Boll. Soc. Geol. It. (Ital. J. Geosci.),* **7,** 297–315.

Patacca, E., Sartori, R. & Scandone, P., 1990. Tyrrhenian basin and Apenninic arcs. Kinematic relations since late Tortonian times, *Mem. Soc. Geol. It.,* **45,** 425–451.

Petit, J-P., 1987. Criteria for the sense of movement on fault surfaces in brittle rocks, *J. Struct. Geo.,* **9,** 597–608.

Pondrelli, S., Salimbeni, S., Ekström, G., Morelli, A., Gasperini, P. & Vannucci, G., 2006. The Italian CMT dataset from 1977 to the present, *Phys. Earth planet. Inter.,* **159**(3–4), 286–303.

Pondrelli, S., Salimbeni, S., Morelli, A., Ekström, G., Postpischl, L., Vannucci, G. & Boschi, E., 2011. European-Mediterranean regional centroid moment tensor catalog: solutions for 2005–2008, *Phys. Earth planet. Inter.,* **185**(3–4), 74–81.

Reasenberg, P.A. & Oppenheimer, D., 1985. FPFIT, FPPLOT and FPPAGE: Fortran computer programs for calculating and displaying earthquake fault-plane solutions, U.S. Geol. Sur., Open-file Report, pp. 85–739.

Rovida, R., Camassi, P., Gasperini, P. & Stucchi, M., eds, 2011. *CPTI11, the 2011 version of the Parametric Catalogue of Italian Earthquakes,* http://emidius.mi.ingv.it/CPTI. doi:10.6092/INGV.IT-CPTI11, Milano, Bologna.

Savage, J.C. & Burford, R.O., 1973. Geodetic determination of relative plate motion in central California, *J. geophys. Res.,* **78,** 832–845.

Sibson, R.H., 1992. Implications of fault-valve behavior for rupture nucleation and recurrence, *Tectonophysics,* **211,** 283–293.

Wells, D.L. & Coppersmith, K.J., 1994. New empirical relationship among magnitude, rupture length, rupture width, rupture area, surface displacement, *Bull. seism. Soc. Am.,* **84,** 974–1002.

Westaway, R. & Jackson, J.A., 1987. The earthquake of 1980 November 23 in Campania-Basilicata (Southern Italy), *Geophys. J. R. astr. Soc.,* **90,** 375–443.